Atlas-Guided Tractography for Segmentation of Striatal Subregions in Early Parkinson's Disease

Iva Bublíková[1], *Tomáš Krajča*[1], *Stanislav Mareček*[2], *Petr Dušek*[2] *and Radim Krupička*[1]

[1]Faculty of Biomedical Engineering, Czech Technical University in Prague, Kladno 272 01, Czech Republic
[2]Department of Neurology and Center of Clinical Neuroscience, First Faculty of Medicine, Charles University and General University Hospital in Prague, Prague 128 21; Czech Republic

Abstract. Parkinson's disease (PD) and isolated REM sleep behaviour disorder (iRBD) are neurodegenerative conditions associated with alterations in the striatum, a subcortical structure essential for motor and cognitive functions. In this study, we apply diffusion tensor imaging (DTI) and probabilistic tractography to segment the striatum into two functionally distinct compartments: striosomes and matrix. A total of 152 subjects were included: 64 PD patients, 47 iRBD patients, and 41 healthy controls. Preprocessing, tractography, and segmentation were performed using the FSL toolbox; voxel-based morphometry (VBM) was used for group comparisons. Probabilistic group atlases were constructed in MNI space and compared with each other and with the standard MNI_152 atlas using RMSE and statistical testing. Results show significant differences in the matrix region, particularly in the right striatum of iRBD subjects compared to both PD and control groups. Our findings suggest that connectivity-based striatal segmentation may reflect early structural changes in neurodegeneration and could support future biomarker development for PD and related disorders. This tractography-based approach offers a promising tool for the personalized analysis of subcortical brain structures in clinical neuroimaging.

1 Introduction

The striatum is a subcortical structure within the basal ganglia, involved in motor control, reward processing, and executive functions [1, 2]. It is composed of the caudate nucleus and putamen and is neurochemically divided into two distinct compartments: the striosomes and the matrix [1, 3]. These compartments differ in embryological origin, connectivity, and vulnerability to neurodegenerative changes [2–4].

Recent studies suggest that PD and iRBD - a prodromal stage of PD - are associated with subtle structural alterations in the striatum, which may precede clinical motor symptoms [5, 6]. Identifying early biomarkers in these regions could enable earlier diagnosis and personalized treatment strategies [7].

DTI and tractography offer a non-invasive approach to assess white matter connectivity and microstructural changes in vivo [8–10]. While traditional striatal segmentation relies on predefined atlases, connectivity-based segmentation via tractography allows for

individualized parcellation reflecting functional subdivisions [8]. This is particularly relevant for mapping the striosome–matrix architecture, previously accessible only through post-mortem or genetically modified models [1].

In this study, we applied a probabilistic tractography-based segmentation method to DTI data from three subject groups: patients with newly diagnosed PD (BIOPD), patients with iRBD, and healthy controls (NORMA). Our aim was to (1) segment the striatum into matrix and striosomal subregions, (2) construct group-specific atlases in MNI space, and (3) compare structural differences across groups and with the standard MNI_152 atlas. We hypothesize that the matrix compartment exhibits significant group-dependent alterations and could serve as a potential structural biomarker for early PD.

2 Methods

This study included a total of 152 participants divided into three groups: 64 patients with newly diagnosed and untreated Parkinson's disease (BIOPD), 47 patients with isolated REM sleep behaviour disorder (iRBD), and 41 neurologically healthy control subjects (NORMA). All participants were recruited through the Department of Neurology, First Faculty of Medicine, Charles University and the General University Hospital in Prague. Diagnosis of iRBD was established using clinical criteria supported by polysomnographic recording. Healthy controls were screened for any neurological or psychiatric disorders, including prodromal symptoms of RBD. All data were fully anonymized prior to analysis in accordance with ethical standards.

2.1 Imaging Acquisition Protocol

Magnetic resonance imaging (MRI) was performed on a Siemens Skyra 3T scanner using a 32-channel head coil. For each subject, diffusion-weighted imaging (DWI) data were acquired in both anterior–posterior (AP) and posterior–anterior (PA) phase encoding directions with a voxel size of 2×2×2 mm, repetition time (TR) of 10.5 ms, and echo time (TE) of 93 ms. High-resolution T1-weighted anatomical images were obtained using an MPRAGE sequence with 1×1×1 mm voxel resolution, TR = 2.2 ms, and TE = 2.43 ms.

Image preprocessing was conducted using tools from the FMRIB Software Library (FSL) [11–13], with the most computationally demanding processes executed on the MetaCentrum distributed computing infrastructure. This included conversion to NIfTI format (*dcm2niix*), correction for susceptibility artifacts and motion (*topup, eddy*), brain extraction (*bet*), intensity normalization (*fslmaths*), and co-registration of diffusion and anatomical images using both linear and nonlinear registration (*flirt, fnirt*). All volumes were resampled to 1 mm isotropic resolution. Quality control was ensured via visual inspection using FSLEyes.

2.2 Segmenting the Striatum

To segment the striatum into striosome-like and matrix-like compartments, we employed a connectivity-based probabilistic tractography approach implemented in FSL. Seed regions were defined in MNI152 space based on the Harvard-Oxford cortical and subcortical atlases, including the posterior orbitofrontal cortex, anterior insula, basolateral amygdala, and mediodorsal thalamic nuclei—regions with known preferential projections to striosomes [44]. The bilateral striatum served as the target region. All anatomical masks were created or edited using *fslmaths*, including the construction of a sagittal midline mask (*-roi*) to constrain tracking to one hemisphere.

The subject-specific processing pipeline involved several transformation steps. First, T1-weighted anatomical images were skull-stripped using *bet* (*-f 0.5 -m -B*) and segmented into tissue types using *fast* (*-t 1 -n 3 -H 0.05 -I 4 -l 20.0*) to generate grey matter masks. Seed and target masks were transformed from standard MNI space to native diffusion space using linear registration (*flirt -omat*) and nonlinear registration (*fnirt* with parameters *--ref, --aff, --refmask, --warpres=4,4,4*). Warp fields were inverted using *invwarp* and optionally combined using *convertwarp* and *--postmat* options.

Probabilistic tractography was performed using *bedpostx* and *probtrackx2*. Tracking was run for each hemisphere independently with 5000 samples per voxel *(--nsamples=5000)*, a step length of 0.5 mm *(--steplength=0.5)*, and curvature threshold of 0.2 *(--c_thresh=0.2)*. The output connectivity maps were thresholded at 0.87 (1.5 SD above mean) and binarized using *fslmaths -thr 0.87 -bin* to produce striosome-like masks. The matrix compartment was obtained by subtracting the striosome mask from the full striatal region (*fslmaths -sub*), and the result was again masked with grey matter segmentation from *fast* to exclude white matter and CSF.

All resulting binary masks (left and right striosome, left and right matrix) were registered to MNI152 space using *applywarp (-i -r -w*) with the subject-specific deformation fields. Masks were post-processed with *fslmaths* for binarization (*-bin*), masking (*-mul*), and thresholding (*-thr 0.5*) prior to atlas creation.

Tractography was performed using *bedpostx*, which estimates the distribution of diffusion parameters at each voxel. Subsequently, *probtrackx2* was used for tracking, with the following key parameters: 5000 samples per voxel (*--nsamples*=5000), step length of 0.5 mm (*--steplength*=0.5), curvature threshold of 0.2 (*--c_thresh*=0.2), and a loop check to prevent anatomically implausible paths (*--loopcheck*). Separate tracking was run for each hemisphere.

The resulting tract density images were thresholded at 0.87 using *fslmaths -thr 0.87 -bin* to retain only highly probable connections. This yielded binary striosome-like masks. The matrix compartment was obtained by subtracting the striosome mask from the full striatal ROI using *fslmaths -sub*, ensuring that both compartments remained mutually exclusive. Tissue-type correction was applied using *fast*-generated segmentation to retain only grey matter voxels within the striatum.

For each subject, four binarized masks were created: left striosome, right striosome, left matrix, and right matrix. These were normalized to MNI space using *applywarp* and deformation fields generated in preprocessing. Normalized masks served as the basis for group-level atlas construction and statistical analysis described in the next section.

2.3 Quantitative Comparison of Connectivity-Based Striatal Atlases

The resulting connectivity profiles were thresholded at 0.87 to isolate strongly connected voxels and binarized to obtain distinct masks for the striosome-like and matrix-like compartments. These masks were then normalized to MNI152 space. Subject-specific segmentations were aggregated to generate group-level probabilistic atlases for BIOPD, iRBD, and NORMA. Quantitative comparisons between group atlases and the standard MNI_152 atlas were performed using mean squared error (MSE) and root mean squared error (RMSE) metrics.

Voxel-wise statistical analyses were conducted using SPM12 and CAT12 [14]. Two-sample t-tests were used to compare the volume and distribution of segmented compartments across groups, with age, sex, and total intracranial volume (TIV) as covariates. A family-wise error (FWE) correction was applied at $p < 0.05$

All resulting masks, atlases, and statistical maps were visually inspected using FSLeyes, which was also used for quality control of image registration and tractography output.

Final visualization of voxel-wise statistical results and anatomical overlays was performed in MRIcroGL, allowing interactive 3D rendering and transparent layering of significant clusters over the MNI152 template. Both tools were essential for visual verification of striatal compartment localization and interpretation of group-level differences.

3 Results

A total of 152 participants were included in the study, comprising 64 patients with Parkinson's disease (BIOPD), 47 patients with isolated REM sleep behavior disorder (iRBD), and 41 healthy controls (NORMA). Descriptive statistics for age and sex distribution are summarized below in Table 1.

Table 1: Demographic characteristics of the study cohorts by sex. (SD = standard deviation)

Group	Sex	*n* =	Mean age (years)	SD (years)	Min age	Max age
BIOPD	F	18	65.11	11.50	37	79
	M	46	57.93	11.76	34	80
	Overall	**64**	**59.95**	**12.05**	**34**	**80**
iRBD	F	7	68.71	2.69	66	73
	M	40	66.75	7.15	47	78
	Overall	**47**	**67.04**	**6.69**	**47**	**78**
NORMA	F	13	58.08	9.00	45	71
	M	28	62.46	8.59	45	81
	Overall	**41**	**61.07**	**8.86**	**45**	**81**

In the BIOPD group, the mean age was 59.95 years (SD = 12.05), with a male predominance (46 men, 18 women). Male participants had a slightly lower average age of 57.93 years compared to 65.11 years in females. Age ranged from 34 to 80 years. The iRBD group also showed a strong male predominance (40 men, 7 women) and had the highest average age across groups at 67.04 years (SD = 6.69). Female participants were slightly older on average than males (68.71 vs. 66.75 years). The age range was 47 to 78 years. The control group (NORMA) consisted of 28 men and 13 women, with a mean age of 61.07 years (SD = 8.86), ranging from 45 to 81 years. Males were older on average (62.46 years) than females (58.08 years). These demographic characteristics reflect the known epidemiology of PD and iRBD, including male predominance and older age in the prodromal group. Age, sex, and total intracranial volume (TIV) were included as covariates in subsequent statistical analyses.

3.1 Tractography-Based Striatal Segmentation

Connectivity-based segmentation of the striatum was successfully performed in all subjects using probabilistic tractography derived from DTI data. Tractographic streamlines connecting the striosome-related seed regions to the striatum in fiber trajectories.

Figure 1 shows a representative example of the tractography output in a healthy control subject. Maximum intensity projections (MIP) in sagittal, axial, and coronal views demonstrate symmetric fiber distributions in both hemispheres, confirming successful modeling of connectivity patterns from striosome-related regions to the striatum.

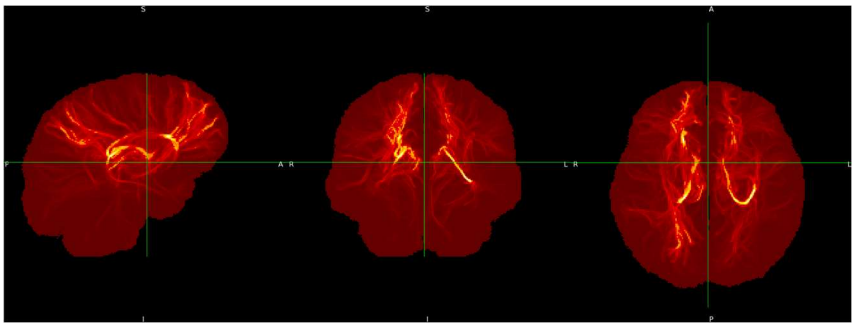

Fig. 1. Maximum intensity projection (MIP) image of probabilistic tractography, shown in sagittal, axial, and coronal views. The image illustrates bilateral fiber pathways in a representative subject, with highest connection densities displayed in yellow colours.

Using the resulting connectivity maps, striosome-like and matrix-like subregions within the striatum were identified by applying a probabilistic threshold (0.87) and binarization. The resulting segmentations were registered to anatomical space and visually verified. An example of the resulting segmentation is shown in Figure 2, where left and right striosomes and matrix regions are clearly separated and color-coded.

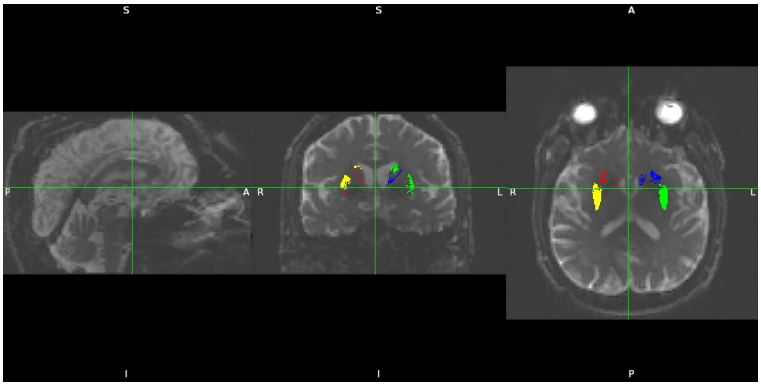

Fig. 2. Tractography-based segmentation of the striatum into functional compartments. The image shows left striosomes (blue), left matrix (green), right striosomes (red), and right matrix (yellow), overlaid on the anatomical MRI in axial, coronal, and sagittal views.

3.2 Probabilistic Atlases

Group-level probabilistic atlases of the striosome and matrix compartments were successfully generated for all three cohorts (BIOPD, iRBD, NORMA). These atlases were created by normalizing subject-specific binary segmentations to MNI152 space and averaging them voxel-wise. The resulting visualisation in 3D rendered atlases (Figure 3) represented the relative probability of voxel inclusion in each compartment across subjects.

Fig. 3. Group-level probabilistic atlases of striatal compartments visualized in 3D for BIOPD (blue), iRBD (orange), and NORMA (red). Atlases are displayed as average masks overlaid on a 3D rendering of the MNI152 brain template.

3.3 Quantitative Comparison to MNI Template

A quantitative comparison was performed using mean squared error (MSE) and root mean squared error (RMSE) between each group-specific atlas and the standard MNI152 reference, as shown in Table 2. The BIOPD group yielded the lowest RMSE values, particularly in the left striatum, suggesting the highest spatial conformity. The iRBD group showed the most significant deviations, particularly in the right matrix, supporting the hypothesis of early pathological changes in prodromal stages of PD.

To further illustrate group-specific differences in striatal segmentation, relative difference maps were computed for each group (as shown in Figure 4**)**. These maps reflect voxel-wise intensity differences in the probabilistic atlases, normalized to their respective group maxima.

Table 2: Mean squared error (MSE) and root mean squared error (RMSE) between group-specific striatal atlases and the MNI152 reference.

Group	Hemisphere	MSE	RMSE
BIOPD	Left	0.4072	0.6381
	Right	0.4398	0.6632
iRBD	Left	0.4470	0.6685
	Right	0.5091	0.7135
NORMA	Left	0.4642	0.6813
	Right	0.4766	0.6903

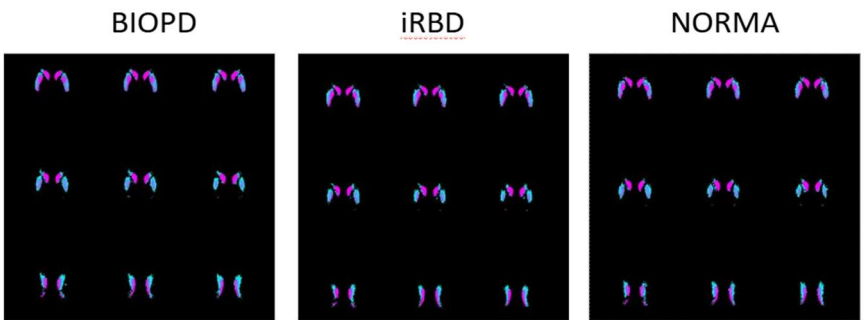

Fig. 4. Relative difference maps of group-specific probabilistic striatal atlases in axial view. Each column represents one cohort: BIOPD (left), iRBD (middle), and NORMA (right). The color scale indicates voxel-wise normalized differences within each atlas, where blue represents the smallest differences and magenta indicates the largest differences.

3.4 Inter-Group Differences in Striatal Compartments

Voxel-wise group comparisons were performed using two-sample t-tests in the CAT12 toolbox, separately for each striatal compartment and hemisphere. Age, sex, and TIV were included as covariates. Results were considered significant at $p < 0.05$, corrected for multiple comparisons using the FWE method. No statistically significant differences were observed in the left hemisphere across any group pairing. Similarly, the striosome-like compartments did not show significant alterations, indicating relatively preserved structural connectivity in these regions across the studied populations. These findings suggest that early disease-related changes may be more localized to the right striatal matrix, which exhibited the most robust and consistent group differences. The following sections summarize the significant results.

3.4.1 BIOPD vs iRBD

A statistically significant difference was found in the right matrix compartment between iRBD and BIOPD groups. Patients with iRBD showed a localized reduction in voxel intensity particularly in the anterior portion of the right striatum. This reduction was interpreted as a decrease in compartment volume or connectivity. This finding was illustrated in the thresholded t-map displayed in Figure 5A.

The group-level Z-score distributions further support this difference, with iRBD subjects exhibiting significantly lower values compared to BIOPD (Figure 5B).

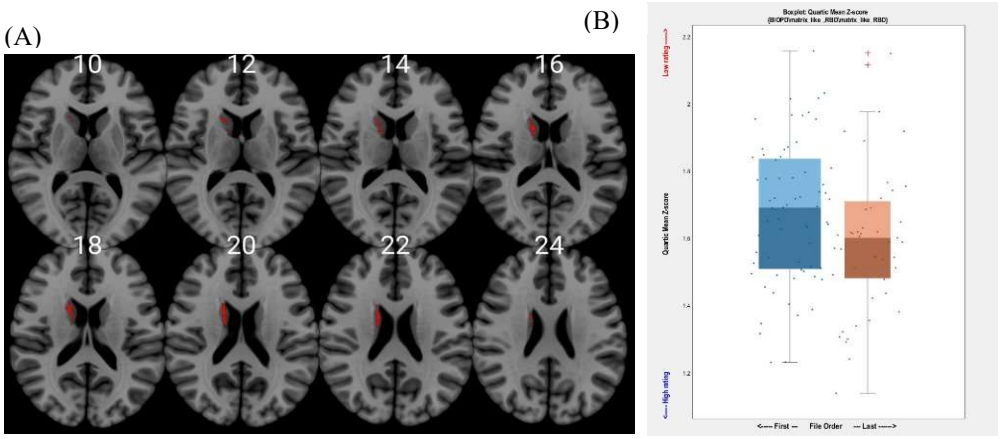

Fig. 5. (A) Voxel-wise statistical comparison between iRBD and BIOPD groups for the right matrix compartment. Significant clusters ($p < 0.05$, FWE-corrected) are shown in red overlaid on the MNI152 template in axial view. **(B)** Boxplot of normalized Z-scores in the right matrix region for BIOPD (blue) and iRBD (orange) groups.

3.4.2 NORMA vs iRBD

Similarly, significant reductions were found in the right matrix of iRBD subjects compared to NORMA. The affected voxels overlapped with those found in the previous comparison, suggesting a consistent vulnerability pattern in the prodromal group. The corresponding t-map is shown in Figure 6A, and boxplot group-level Z-score distributions are illustrated in Figure 6B.

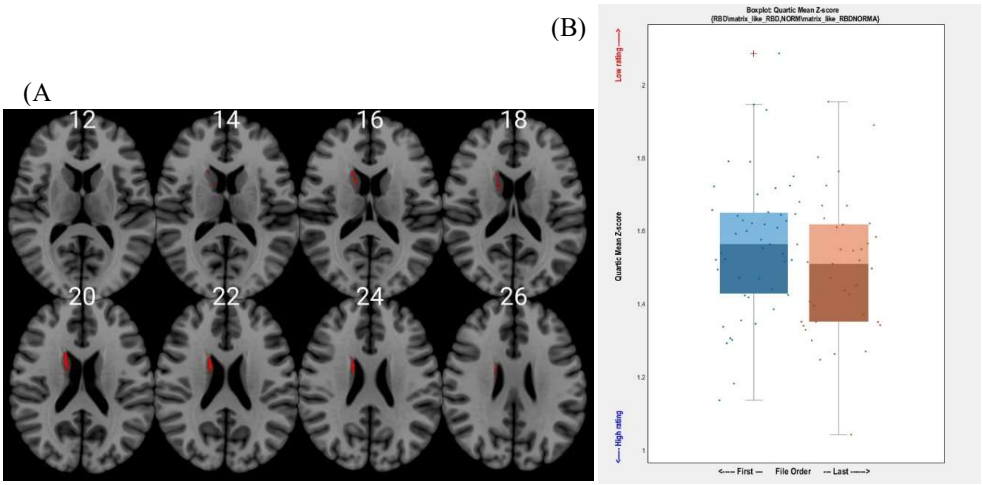

Fig. 6. (A) Statistical map of voxel-wise differences in the right matrix between iRBD and NORMA in red. Highlighted regions indicate significant reductions in the iRBD group. **(B)** Boxplot comparison of Z-scores in the right matrix compartment for iRBD (blue) and NORMA (orange) groups.

4 Discussion

This study demonstrated the feasibility and value of using diffusion tensor imaging and probabilistic tractography for segmenting the striatum into functionally distinct compartments—striosome-like and matrix-like—and for comparing these compartments across clinically relevant cohorts. The results revealed consistent differences in the right matrix compartment between iRBD and both BIOPD and healthy control groups, supporting the hypothesis that early neurodegenerative changes may first emerge in this subregion. This may reflect early compensatory responses to dopaminergic neuron loss—such as localized hyperplasia or hypertrophy within striatal subregions at different disease stages.

These findings are in line with recent work by Funk et al. [15], who used advanced probabilistic tractography to show that striosome and matrix compartments have distinct projections to globus pallidus internus (GPi) and thalamic nuclei, with matrix pathways being 5.7 times more likely to reach the GPi. This supports the view that the matrix compartment plays a more prominent role in motor circuit regulation, which may explain why it appears more vulnerable in the prodromal phase of PD (iRBD group). Moreover, the observed asymmetry—statistical differences occurring only in the right matrix—aligns with the concept of lateralized vulnerability in neurodegeneration and raises questions about underlying hemispheric specializations. In right-handed individuals, the right hemisphere may be structurally or functionally less dominant than the left (as controlling the non-dominant side), potentially contributing to these right-sided alterations. An updated follow-up by Funk et al. [16] confirmed these findings using higher-resolution data and more advanced tractography pipelines, reinforcing the functional importance and anatomical vulnerability of the matrix compartment.

Interestingly, no significant differences were detected in the striosomal compartments, consistent with the findings of Waugh et al. [17], who demonstrated that in vivo MRI-based striosome segmentation remains more challenging and yields lower variability across populations. The stability of the striosome structure may also relate to its association with limbic circuits, which are typically affected later in Parkinsonian syndromes.

The methodological approach used here builds upon previous diffusion-based parcellation strategies but extends them by combining voxel-wise statistical analysis with

group-level probabilistic atlases, offering a population-based template for future studies. Importantly, the matrix compartment differences between iRBD and BIOPD suggest that connectivity-based segmentation could be a sensitive imaging biomarker for early-stage PD.

The present study is subject to several limitations. First, there is a pronounced gender imbalance in the iRBD cohort (40 males vs. 7 females), which may constrain the generalizability of the findings. Second, the predominance of right-handed people worldwide [18] potentially may results in unilateral differences in the right hemisphere. Future work should focus on longitudinal validation of these findings, exploring whether the observed matrix alterations in iRBD predict conversion to PD. Furthermore, subsequent studies should employ more equitable samples regarding gender and consider the role of handedness as a potential covariate in the analysis. In addition, integrating imaging modalities may clarify the significance of the observed structural differences.

5 Conclusion

This study presents a tractography-based approach for segmenting the striatum into striosome-like and matrix-like compartments, and demonstrates its potential for detecting early structural alterations in neurodegenerative conditions. Using group-level probabilistic atlases and voxel-wise analysis, we identified significant differences in the right matrix compartment of iRBD subjects compared to both PD patients and healthy controls. These findings support the hypothesis that matrix alterations precede motor symptom onset and may serve as a structural biomarker for prodromal PD. The proposed method offers a reproducible and data-driven framework for studying basal ganglia organization, with potential clinical applications in early diagnosis and patient stratification. Future studies should validate these results longitudinally and expand toward multimodal integration to better understand the functional consequences of striatal connectivity changes.

6 Acknowledgment

This research was funded by the National Institute for Neurological Research (Programme EXCELES, ID Project No. LX22NPO5107)–Financed by the European Union–Next Generation EU, and was supported by the Grant Agency of the Czech Technical University in Prague, grant No. SGS25/187/OHK4/3T/17.
Computational resources were provided by the e-INFRA CZ project (ID:90254), supported by the Ministry of Education, Youth and Sports of the Czech Republic. Access to CESNET storage facilities provided by the project “e-INFRA CZ” under the programme “Projects of Large Research, Development, and Innovations Infrastructures” LM2018140).

7 Resources

1. Brimblecombe KR, Cragg SJ (2017) The Striosome and Matrix Compartments of the Striatum: A Path through the Labyrinth from Neurochemistry toward Function. ACS Chem Neurosci 8:235–242. https://doi.org/10.1021/acschemneuro.6b00333
2. Cirillo G, Caiazzo G, Franza F, et al (2025) Evidence for direct dopaminergic connections between substantia nigra pars compacta and thalamus in young healthy humans. Front Neural Circuits 18:. https://doi.org/10.3389/fncir.2024.1522421
3. Miller DR, Guenther DT, Maurer AP, et al (2021) Dopamine Transporter Is a Master Regulator of Dopaminergic Neural Network Connectivity. J Neurosci 41:5453–5470. https://doi.org/10.1523/jneurosci.0223-21.2021

4. Beier KT, Steinberg EE, DeLoach KE, et al (2015) Circuit Architecture of VTA Dopamine Neurons Revealed by Systematic Input-Output Mapping. Cell 162:622–634. https://doi.org/10.1016/j.cell.2015.07.015
5. Bramich S, King A, Kuruvilla M, et al (2022) Isolated REM sleep behaviour disorder: current diagnostic procedures and emerging new technologies. J Neurol 269:4684–4695. https://doi.org/10.1007/s00415-022-11213-9
6. Peřinová P, Plchová L, Bušková J, et al (2018) Patients with idiopathic REM sleep behavior disorder follow-up – phenoconversion into parkinsonian syndrome and dementia. Cesk Slov Neurol N 81/114:205–207. https://doi.org/10.14735/amcsnn2018205
7. Búřil J, Búřilová P, Pokorná A, et al (2020) Patient with Parkinson‘s disease in data sources of the National Health Information System. Cesk Slov Neurol N 83/116:550–554. https://doi.org/10.14735/amcsnn2020550
8. Reid AT, Camilleri JA, Hoffstaedter F, Eickhoff SB (2022) Tract-specific statistics based on diffusion-weighted probabilistic tractography. Commun Biol 5:. https://doi.org/10.1038/s42003-022-03073-w
9. Le Bihan D, Turner R, Douek P, Patronas N (1992) Diffusion MR imaging: clinical applications. American Journal of Roentgenology 159:591–599. https://doi.org/10.2214/ajr.159.3.1503032
10. Shepherd TM, Hoch MJ (2022) MRI-Visible Anatomy of the Brainstem. Neuroimaging Clinics of North America 32:553–564. https://doi.org/10.1016/j.nic.2022.04.003
11. Smith SM, Jenkinson M, Woolrich MW, et al (2004) Advances in functional and structural MR image analysis and implementation as FSL. Neuroimage 23 Suppl 1:S208-219. https://doi.org/10.1016/j.neuroimage.2004.07.051
12. Jenkinson M, Beckmann CF, Behrens TEJ, et al (2012) FSL. Neuroimage 62:782–790. https://doi.org/10.1016/j.neuroimage.2011.09.015
13. Woolrich MW, Jbabdi S, Patenaude B, et al (2009) Bayesian analysis of neuroimaging data in FSL. Neuroimage 45:S173-186. https://doi.org/10.1016/j.neuroimage.2008.10.055
14. Gaser C, Dahnke R, Thompson PM, et al (2023) CAT – A Computational Anatomy Toolbox for the Analysis of Structural MRI Data. bioRxiv 2022.06.11.495736. https://doi.org/10.1101/2022.06.11.495736
15. Funk AT, Hassan AAO, Brüggemann N, et al (2023) In humans, striato-pallido-thalamic projections are largely segregated by their origin in either the striosome-like or matrix-like compartments. Front Neurosci 17:. https://doi.org/10.3389/fnins.2023.1178473
16. Funk A, Hassan A, Waugh J (2024) In humans, insulo-striate structural connectivity is largely biased toward either striosome-like or matrix-like striatal compartments
17. Waugh J, Hassan A, Kuster J, et al (2022) An MRI method for parcellating the human striatum into matrix and striosome compartments in vivo. NeuroImage 246:118714. https://doi.org/10.1016/j.neuroimage.2021.118714
18. Vuoksimaa E, Koskenvuo M, Rose RJ, Kaprio J (2009) Origins of Handedness: A nationwide study of 30161 adults. Neuropsychologia 47:1294–1301. https://doi.org/10.1016/j.neuropsychologia.2009.01.007